Physics of Plasmas

Parameter interval optimization of the DBD plasma actuator based on orthogonal experiment and RBF neural network approximation model

Cite as: Phys. Plasmas **28**, 023504 (2021); https://doi.org/10.1063/5.0037035
Submitted: 11 November 2020 . Accepted: 14 January 2021 . Published Online: 02 February 2021

Yanghui Zhang, Xingjun Hu, Zheng Hui, Yichen Liu, Zhiqiang Zhang, and Jingyu Wang

Parameter interval optimization of the DBD plasma actuator based on orthogonal experiment and RBF neural network approximation model

Cite as: Phys. Plasmas **28**, 023504 (2021); doi: 10.1063/5.0037035
Submitted: 11 November 2020 · Accepted: 14 January 2021 ·
Published Online: 2 February 2021

View Online Export Citation CrossMark

Yanghui Zhang,[1] Xingjun Hu,[1] Zheng Hui,[2] Yichen Liu,[1] Zhiqiang Zhang,[1] and Jingyu Wang[1,a)]

AFFILIATIONS

[1]State Key Laboratory of Automobile Simulation and Control, Jilin University, Changchun 130025, China
[2]Automobile Research Institute of China Heavy Duty Automobile Group Co, Ltd., Jinan 250031, China

[a)]Author to whom correspondence should be addressed: wangjy@jlu.edu.cn

ABSTRACT

To further improve the performance of the dielectric barrier discharge-plasma actuator (DBD-PA) and to ensure the convenience of excitation intensity adjustment, the parameters of the DBD-PA were subjected to interval optimization on the basis of an orthogonal experiment and the radial basis function (RBF) neural network approximation model. The parameters of the DBD-PA included electrode gap d1, exposed electrode width d2, covered electrode width d3, frequency f, and voltage peak-to-peak value Vpp. The maximum velocity U_{max} induced by DBD-PA was taken as the target variable. Orthogonal analysis results showed that the influence of Vpp on U_{max} was highly significant, whereas d1 had some influence and the other three parameters' influence was not significant. On the basis of the orthogonal experiment results, an RBF neural network approximate model was established. Through two groups of randomized experiments, the prediction error of the approximate model is verified to be within 3%. The interval optimization algorithm was used to optimize the parameters of the DBD-PA with Vpp as the uncertain variable. The optimal parameter combination of deterministic variables obtained by optimization is d1 = 0 mm, d2 = 13 mm, d3 = 20 mm, and f = 8.6 kHz. Under different Vpp, the performance of the DBD-PA greatly improved in the optimal parameter combination, and the average increase in U_{max} was about 0.52 m/s.

I. INTRODUCTION

In accordance with the generation mode of plasma, a plasma actuator (PA) can be divided into the following types:[1] laser-induced plasma, corona discharge plasma, arc discharge plasma, and dielectric barrier discharge (DBD) plasma. With its advantages of a simple structure, stable operation, and rapid response,[2] DBD-PA has become a research hotspot in the field of wing separation flow control,[3–6] boundary layer transition control,[7–9] backward-facing step separation flow control,[10–12] and aerodynamic noise control.[13,14] As shown in Fig. 1, the typical DBD-PA structure mainly includes the exposed electrode, the covered electrode, and the electrodes separated by a dielectric layer.[15] The air on the surface of the actuator breaks down under the effect of the high voltage, and ionized ions move under the drive of electric field and collide with neutral gas molecules to transfer energy, thus inducing airflow acceleration near the wall and generating ionic wind.[16]

Previously, many scholars used single-factor parameter experiment method to improve the performance of the DBD-PA.[17–21] Forte *et al.*[17] performed a parametric study that includes electrode gap, covered electrode width, frequency, voltage amplitude, material permittivity, and dielectric layer thickness to increase the velocity of the ionic wind induced by DBD-PA. Thomas *et al.*[18] studied the effects of dielectric material and thickness, applied voltage amplitude and frequency, voltage waveform, exposed electrode geometry, and covered electrode width on the body force produced by a single DBD-PA. Xiaohua *et al.*[19] studied the effects of covered electrode width on the DBD-PA performance and showed that the velocity of the ionic wind increased with the covered electrode width. Guoqiang *et al.*[20] proved that the maximum velocity of the induced airflow by DBD-PA increases with the applied voltage amplitude and frequency. The sample space of the single-factor parametric experiment method is not uniform, and the optimal parameter combination of the actuator obtained by the optimization algorithm may not have the best performance.

When DBD-PA is used for flow control, different excitation intensity is required to achieve the best control effect under different working conditions. When the excitation intensity exceeds the threshold needed for the optimal control effect, the control effect will not

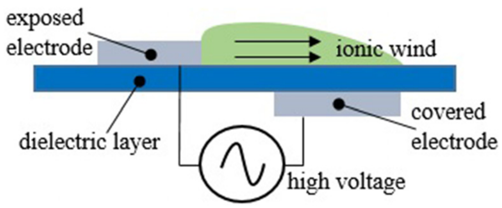

FIG. 1. Typical DBD-PA structure.

increase with the increase in the excitation intensity. When Zheng[15] applied DBD-PA to control the separation flows of the Ahmed model, which is a standard simplified model used for automotive aerodynamics research, the low excitation intensity could achieve the best drag reduction rate when the incoming flow speed was low, and the drag coefficient would not decrease with the increase in excitation voltage. When the incoming flow speed was high, the maximum excitation intensity did not reach the best drag reduction rate. When Kopiev *et al.*[14] applied high-frequency DBD-PA to control the cylinder separation noise, after the excitation intensity reaches the optimal noise reduction threshold, cylinder separation noise will also no longer decrease with the increase in excitation intensity. Therefore, when DBD-PA is applied for flow control, the performance of actuator should be improved and the excitation intensity should be adjusted conveniently. Adjusting all parameters in the flow control experiment will result in a very heavy workload.

In order to further improve the performance of the DBD-PA and to ensure the convenience of the excitation intensity adjustment, the parameters of the DBD-PA were subjected to interval optimization on the basis of an orthogonal experiment and the radial basis function (RBF) neural network approximation model. On the basis of previous single-factor parameter experiment results, this paper selected electrode gap d1, exposed electrode width d2, covered electrode width d3, frequency f, and voltage peak-to-peak value Vpp as design variables and adopted the orthogonal array method for experimental design. With U_{max} as the target variable, which is the maximum value in the time-averaged velocity field measured by two-dimensional particle image velocimetry (2D-PIV), the significance of each parameter on the performance of the DBD-PA was studied by orthogonal analysis. On the basis of the results of orthogonal experiments, an approximate model of the radial basis function (RBF) neural network was established to fit the relationship between the parameters of the actuator and the target variables, and the influence trend of each parameter on the performance of the DBD-PA was described. The interval optimization algorithm was adopted to find the optimal combination of the uncertainty variables by taking the parameters with relatively significant influence as the uncertainty variable, the parameters with insignificant influence as the certainty variable, and U_{max} as the uncertainty objective function so that the DBD-PA has better performance when the uncertainty variable changes. When DBD-PA is used for a flow control experiment, only the uncertainty variables are adjusted to achieve different excitation intensity, which improves not only the performance of the DBD-PA but also the convenience of excitation intensity adjustment.

II. EXPERIMENTAL SETUP

In this paper, Nanjing Suman Plasma Technology Co., Ltd. (CTP-2000K) is used to output sinusoidal AC voltage with Vpp of

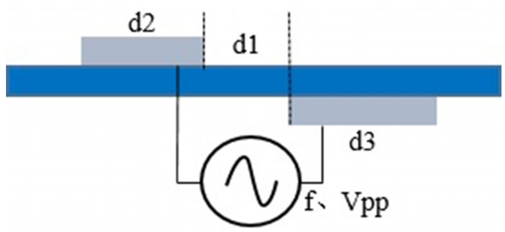

FIG. 2. Parameters of DBD-PA.

0–30 kV, frequency adjustable range of 5–20 kHz, central frequency of 10 kHz, and maximum power of 500 W. The parameters of DBD-PA studied in this paper are shown in Fig. 2, including electrode gap d1, exposed electrode width d2, covered electrode width d3, frequency f, and voltage peak-to-peak value Vpp. The values of DBD-PA parameters are shown in Table I. The DBD-PA is 190 mm in length and is placed on a 15-mm-thick high-temperature-resistant epoxy plate. Copper foil tape with a thickness of 0.05 mm was used for the electrodes. Ten layers of polyimide film with a dielectric constant ε_r of 3.5 and thickness of 0.05 mm were used for dielectric layer.

In this paper, two-dimensional particle image velocimetry (2D-PIV) is used to measure the induced velocity of DBD-PA. This technology has the advantages of noncontact measurement, noninterference with the flow field, and high measurement accuracy.[15] The laser has a wavelength of 532 nm and a maximum laser energy of 200 mJ. The CCD camera has a resolution of 1024×1280 pixels and an image acquisition frequency of 4 Hz. The CCD camera uses a microfocal-length lens to improve the resolution. A narrow-band filter is added to the lens to reduce wall reflection. The tracer particles are volatilized by heating liquid paraffin. The particles have a uniform diameter and long residence time in the air. Fast Fourier transform cross-correlation algorithm is used to calculate the particle velocity in the interpretation area. The time-averaged velocity field was obtained by taking 300 sets of vector images continuously.

III. RESULTS AND DISCUSSIONS

A. Experimental design and measurement results

Common experimental design methods include single-factor parameter experiment method, full-factor design method, optimal Latin hypercube design method, and orthogonal array method. The parameter experiment method studies only the influence of each factor on the experimental results when it is independent of other factors and applies only to the case where the interaction influence is not significant. The full-factor design method is expensive because it involves all combinations of all factors at all levels. The optimal Latin hypercube

TABLE I. Values of DBD-PA parameters.

d1/mm	d2/mm	d3/mm	f/kHz	Vpp/kV
0	5	10	8.6	12
1	8	13	8.8	14
2	10	17	9.0	16
3	13	20	9.2	18

TABLE II. Orthogonal table and measurement results of U_{max}.

Run	d1/mm	d2/mm	d3/mm	f/kHz	Vpp/kV	U_{max}/m·s^{-1}
1	0	5	10	8.6	12	2.05
2	0	8	13	8.8	14	2.60
3	0	10	17	9.0	16	3.04
4	0	13	20	9.2	18	4.39
			……			
29	3	5	17	9.2	14	2.77
30	3	8	20	9.0	12	0.68
31	3	10	10	8.8	18	2.94
32	3	13	13	8.6	16	2.41

design method requires many levels of each factor, which is difficult to implement for DBD-PA. The orthogonal array method can greatly reduce the number of experiments and ensure the orthogonality of experimental sample points. The requirement of factor level number is also easy to implement for DBD-PA. Therefore, the orthogonal array method is adopted in this paper for experimental design. The structure of the orthogonal table is generally expressed as $L_p(n^m)$, where p denotes the number of experiments, m denotes the number of factors, and n denotes the level number of factors. In this paper, an orthogonal table of five factors and four levels is used. The orthogonal table and measurement results of U_{max} induced by the DBD-PA are shown in Table II. Run1, combined with the minimum values of each parameter, is set as the base parameter combination to compare the optimization result.

The time-averaged velocity fields induced by the DBD-PA in the near-wall region of Run1–3 are shown in Fig. 3. The origin of the coordinate system is taken as the end of exposed electrode on the surface of the insulating layer on the longitudinal symmetric surface. The DBD-PA forms an obvious acceleration region near the wall. The ambient air flows to the plasma region and is gradually accelerated. In the downstream of the actuator, as the plasma concentration decreases, the thrust generated gradually decreases until it disappears, and the airflow gradually slows down and diffuses in the direction of height. The distribution of flow velocity induced by DBD-PA along the z-direction at x = 10 mm is shown in Fig. 4. The airflow acceleration area is mainly located within the range of 2 mm from the wall surface, and the maximum velocity occurs at a position about 0.7 mm from the wall surface.

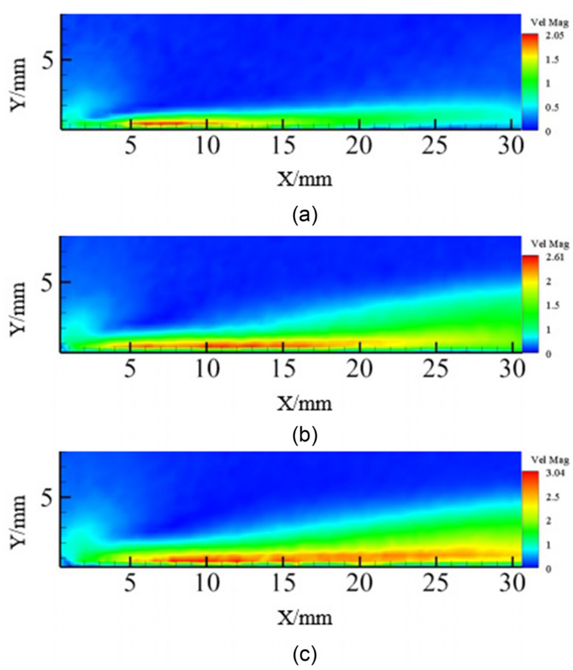

FIG. 3. Time-averaged velocity fields: (a) Run1, (b) Run2, and (c) Run3.

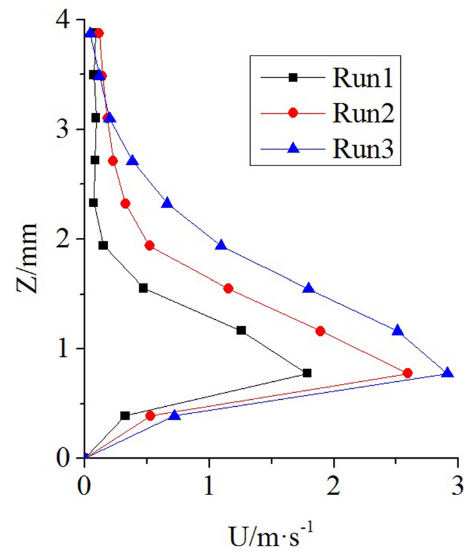

FIG. 4. Distribution of flow velocity at x = 10 mm of Runs1–3.

B. Orthogonal analysis

In this part, range analysis and variance analysis are performed on the results of orthogonal experiments to analyze the significance of the influence of each parameter on U_{max}.

Range analysis, which is also known as intuitive analysis, calculates the range of each factor to analyze its impact on the experimental results. The arithmetic mean value of the experimental results corresponding to the level i of factor j is expressed as K_{ij}. Range R_j is expressed as the difference between the maximum and minimum values of K_{ij} corresponding to factor j.[22] Range R_j can directly reflect the influence of factor j on the experimental results. A great range R_j corresponds to the great influence of factor j on the experimental results. The range calculation results are shown in Table III. The parameter

TABLE III. Range calculation results.

Parameters	d1	d2	d3	f	Vpp
R_j/m·s^{-1}	0.70	0.44	0.44	0.30	1.95

TABLE IV. Variance calculation results.

Parameters	SS_j	f_j	F	Critical value
d1	0.32	3	6.34	$F_{0.1}(3,3) = 5.391$
d2	0.13	3	2.61	
d3	0.16	3	3.28	$F_{0.05}(3,3) = 9.28$
f	0.05	3	1.00	
Vpp	2.11	3	42.09	$F_{0.01}(3,3) = 29.457$
Error	0.05	3		

that has the greatest influence on U_{max} is Vpp, while d1 has a secondary influence, and d2, d3, f have little influence on U_{max}.

The variance analysis method is also known as the F-test method, and its accuracy is relatively high because it amplifies the numerical fluctuation of the calculation results.[23] The statistic F selected in the analysis of variance is as follows:

$$F = \frac{\frac{SS_j}{f_j}}{\frac{SS_e}{f_e}}, \tag{1}$$

where SS_j is the deviation sum of squares of factor j; f_j is the degree of freedom of factor j; SS_e is the deviation sum of squares of error; f_e is the degree of freedom of error; SS_e is the minimum value in SS_j.[24] The calculation method of SS_j and f_j is as follows:

$$SS_j = \sum_{i=1}^{n} \left(K_{ij} - \frac{\sum_{i=1}^{n} K_{ij}}{n} \right)^2, \tag{2}$$

$$f_j = n - 1. \tag{3}$$

The results of variance calculation are shown in Table IV. Compared with the critical value of F, Vpp has a highly significant influence on U_{max}, while d1 has a certain influence, and the other three factors have no significant influence. The results are basically consistent with those obtained by the range analysis method.

C. Establishing the RBF neural network approximate model

Compared with other approximate models, the RBF neural network approximation model has the advantages of no mathematical assumption, strong fault-tolerant function, and fast learning speed, and it has been widely applied in many fields. On the basis of the orthogonal experiment results in the previous part, an RBF neural network approximation model was established to fit the relationship between the design variables and the target variable, and the fitting effect is shown in Fig. 5. To test the fitting accuracy of the approximate model, two groups of parameters were randomly selected for verification experiment. The measurement results of induced maximum velocity are shown in Table V, and the error of both groups is within 3%, which proves that the approximate model has achieved good fitting accuracy.

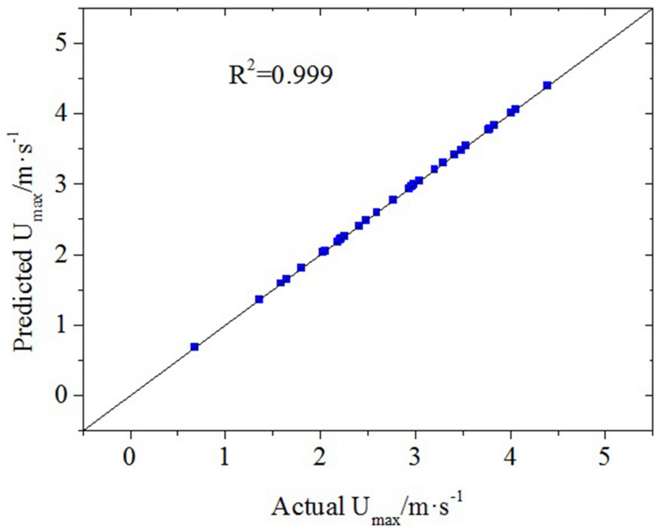

FIG. 5. Fitting effect of the RBF neural network approximation model.

On the basis of the RBF neural network approximation model, the influence trend of each parameter on U_{max} was analyzed briefly by selecting some parameter combinations. As can be seen from Fig. 6, U_{max} gradually decreases as d1 increases. With a bigger gap, the electric field falls down because the effective dielectric thickness between the electrodes increases.[15,17] As can be seen from Fig. 7, when d2 increases from 5 mm to 10 mm, U_{max} gradually decreases, but it remains basically unchanged when d2 increases from 10 mm to 13 mm. This result was obtained because when the exposed electrode is narrow, the downstream electric field intensity is larger than the threshold and more electrons are generated at the same time, thereby improving the coverage of high-density electrons near the wall and becoming conducive to the discharge of the DBD-PA.[25] When d2 exceeds 10 mm, the increase in the upstream electrode width of the actuator has little effect on the electric field intensity.

Figure 8 shows that at low voltage (Vpp = 12–16 kV), U_{max} does not change with the change in d3. At high voltage (Vpp = 16–18 kV), U_{max} increases with the increase in d3, and the growth speed decreases

TABLE V. Verification of the RBF neural network approximate model.

						U_{max}/m·s^{-1}		
Parameters	d1/mm	d2/mm	d3/mm	f/kHz	Vpp/kV	Actual	Predicted	Error
Test-1	1	8	13	8.8	14	2.554	2.531	0.1%
Test-2	1	10	20	8.6	16	3.672	3.591	2.2%

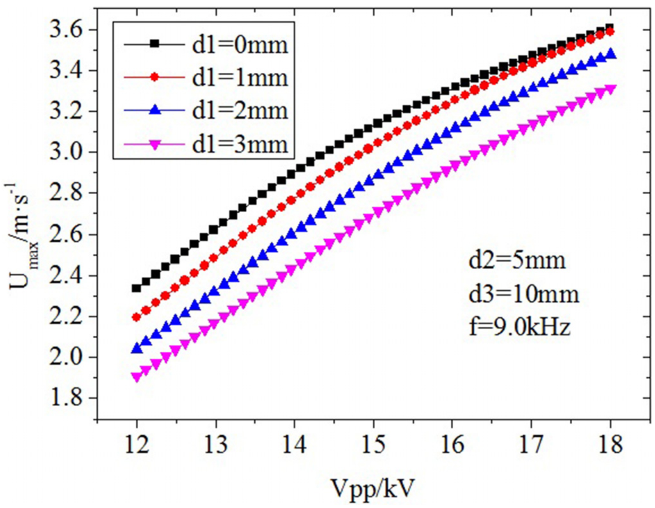

FIG. 6. Influence of d1 on U_{max}.

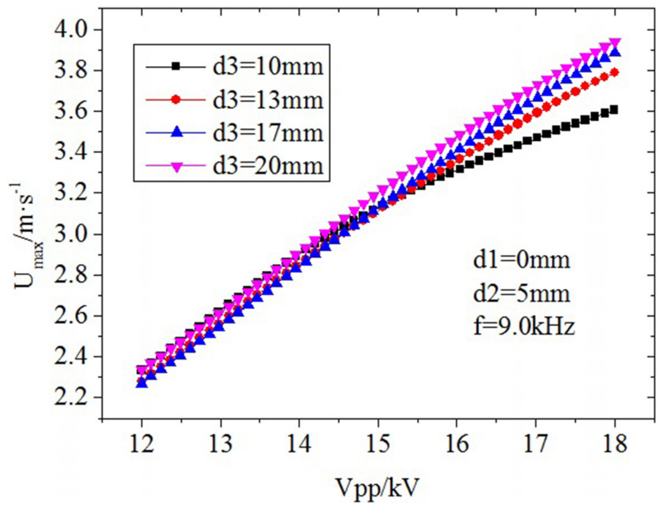

FIG. 8. Influence of d3 on U_{max}.

gradually. When Vpp is high, the generated plasma area is larger. The wider the covered electrode is, the farther the electric field is extended, and the airflow can be accelerated over a longer distance.[17–19] When Vpp is low, the generated plasma area does not reach the width of the covered electrode, so the variation of d3 has no effect on U_{max}. Figure 9 shows that, consistent with the results of orthogonal analysis, f has basically no influence on U_{max}. As can be seen from Figs. 6–9, with the increase in Vpp, the electric field intensity increased significantly, and U_{max} increased significantly.

D. Interval optimization

For the minimization (or maximization) problem, the purpose of the interval optimization algorithm is to find the optimal combination of the certain variables when the uncertain variables change within the value range to minimize the midpoint (or maximum) and the interval radius of the uncertainty objective function.[26]

According to Sec. III B, Vpp has a significant impact on the performance of the DBD-PA, while the remaining four parameters have no significant impact. Therefore, Vpp is taken as the uncertain variable; d1, d2, d3, and f are used as the certain variables; and U_{max} is taken as the uncertain objective function to find the optimal combination of the certain variables so that the actuator has better performance when Vpp changes. On the basis of the interval optimization principle, the interval optimization procedure in this paper is as follows:

(1) To facilitate the application of DBD-PA for flow control in the experiment, the parameters of the actuator are discretized within the value range. The value range and distance between the values of each parameter are shown in Table VI. Full-factor

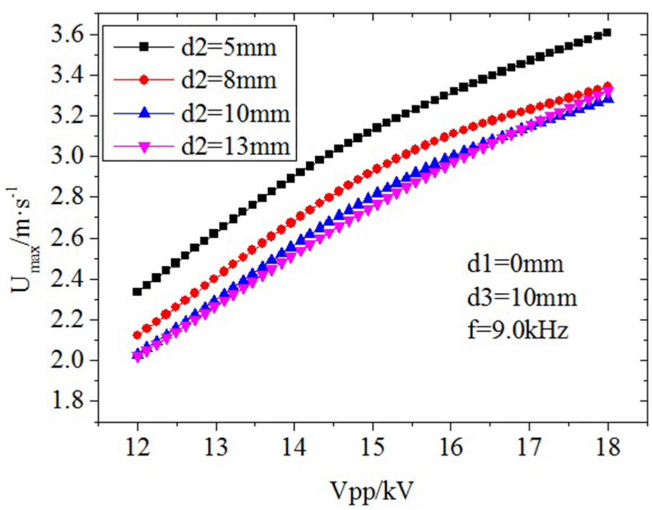

FIG. 7. Influence of d2 on U_{max}.

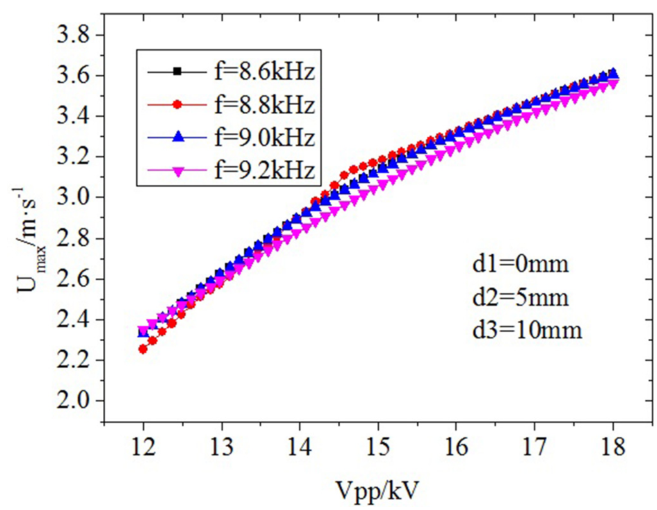

FIG. 9. Influence of f on U_{max}.

experimental design is performed for certain variables d1, d2, d3, and f to obtain the interval optimized sample space. To turn the maximization problem into the minimization problem, the target variable U_{max} is taken to the negative and called Y. With the application of the RBF approximation model, when Vpp changes within the value range, the variation range of Y [Ymin, Ymax] of each group of sample points is obtained.

(2) The midpoint Y_m and the interval radius Y_w are calculated for each set of sample points

$$Y_m = \frac{Y_{\max} + Y_{\min}}{2}, \tag{4}$$

$$Y_w = \frac{Y_{\max} - Y_{\min}}{2}. \tag{5}$$

(3) Y_m and Y_w are regularized and linearly weighted[24]

$$f = \frac{\alpha Y_m}{\emptyset} + \frac{(1-\alpha) Y_w}{\varphi}, \tag{6}$$

$$\emptyset = \min|Y_m|, \quad \varphi = \min|Y_w|, \tag{7}$$

where α is the weight coefficient; $\emptyset$ and φ are regularization coefficients, which are used to avoid the order of magnitude difference between Y_m and Y_w.[24]

(4) At this point, the interval optimization problem is transformed into a certain optimization problem, that is, to find the minimum value of the objective function *f* in the sample space. In order to obtain better performance of the DBD-PA, the weight coefficient α is set as 0.6, 07, and 0.8, respectively. The optimal and base parameter combination is shown in Table VII. When the weight coefficient α is taken for each value, the parameter combination obtained by optimization always is: d1 = 0 mm, d2 = 13 mm, d3 = 20 mm, and f = 8.6 kHz, so this parameter combination is determined to be the final optimization result. The comparison of U_{max} under different Vpp between the optimal and base parameter combination is shown in Fig. 10. Under different Vpp, the performance of the DBD-PA greatly improved when the optimal parameter combination was applied, and U_{max} increased by 0.52 m/s on average.

IV. CONCLUSION

To improve the performance of the DBD-PA and to ensure convenient excitation intensity adjustment, the parameters of the DBD-PA were subjected to interval optimization on the basis of the orthogonal experiment and the RBF neural network approximation model. The conclusions are as follows:

TABLE VI. Value range and distance between the values of each parameter.

Parameters	Range	Interval
d1/mm	0–3	1
d2/mm	5–13	1
d3/mm	10–20	1
f/kHz	8.6–9.2	0.1
Vpp/kV	12–18	0.12

TABLE VII. Optimal and base parameter combination.

Parameters	d1/mm	d2/mm	d3/mm	f/kHz
$\alpha = 0.6$	0	13	20	8.6
$\alpha = 0.7$	0	13	20	8.6
$\alpha = 0.8$	0	13	20	8.6
Base	0	5	10	8.6

(1) The flow field induced by DBD-PA in a windless environment was measured by 2D-PIV. The time-average velocity fields of Runs1–3 show that the airflow acceleration area formed by the DBD-PA near the wall is mainly located within 2 mm from the wall, and the maximum velocity appears at a position about 0.7 mm from the wall.

(2) The results obtained by the range analysis method and variance analysis method are basically consistent: Vpp has a significant effect on the performance of the actuator, d1 has a certain effect, and the other three parameters have no significant effect.

(3) On the basis of the results of orthogonal experiments, an approximate model of RBF neural network was established to fit the relationship between the parameters of the actuator and U_{max}. Through two groups of randomized experiments, the prediction error of the approximate model is verified to be within 3%, which has a good fitting accuracy.

(4) On the basis of the RBF neural network approximation model, the influence trend of each parameter on U_{max} was analyzed briefly by selecting some parameter combinations. With the increase in d1, U_{max} decreases gradually. When d2 increases from 5 mm to 10 mm, U_{max} gradually decreases, but when d2 increases from 10 mm to 13 mm, U_{max} remains basically unchanged. When Vpp = 12–16 kV, U_{max} does not change with the change in d3; when Vpp = 16–18 kV, U_{max} increases with the increase in d3, and the growth speed decreases

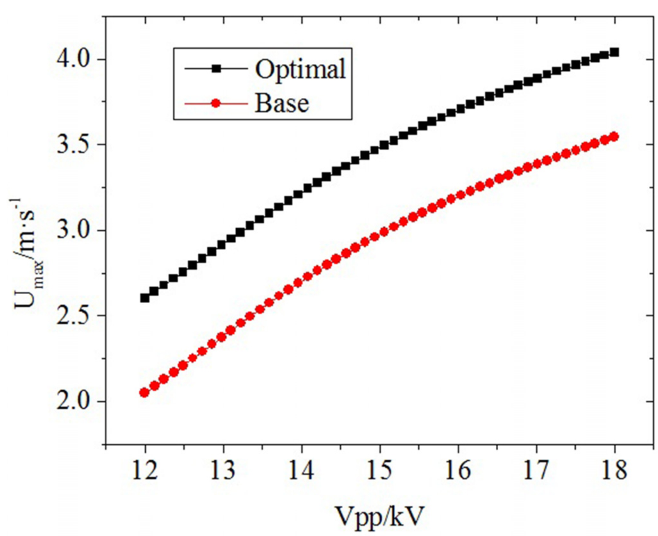

FIG. 10. Comparison of U_{max} under different Vpp.

gradually. The frequency f has basically no influence on U_{max}. With the increase in Vpp, U_{max} increased significantly.

(5) The interval optimization algorithm was used to optimize the parameters of the actuator. The optimal parameter combination obtained by interval optimization is $d1 = 0\,mm$, $d2 = 13\,mm$, $d3 = 20\,mm$, and $f = 8.6\,kHz$. Under different Vpp, the performance of the DBD-PA greatly improved when the optimal parameter combination was applied, and U_{max} increased by 0.52 m/s on average.

ACKNOWLEDGMENTS

This work was supported by the National Nature Science Foundation of China under Contract No. 51875238.

DATA AVAILABILITY

The data that support the findings of this study are available from the corresponding author upon reasonable request.

REFERENCES

[1] D. Hai, *Nanosecond Pulse Dielectric Barrier Discharge Plasma Actuator Flow Control Mechanisms and Application* (College of Aerospace Engineering, Nanjing University of Aeronautics and Astronautics, Nanjing, 2016).

[2] Z. Xin, H. Yong, Y. Pengyu, T. Kun, and L. Huaxing, "Investigation on the turbulent characteristics of the jet induced by a plasma actuator," Chin. J. Theor. Appl. Mech. **50**(4), 776–786 (2018).

[3] C. Durasiewicz, A. Singh, and J. Little, "A comparative flow physics study of Ns-DBD vs Ac-DBD plasma actuators for transient separation control on a NACA 0012 airfoil," AIAA Paper No. 2018-1061.

[4] A. Kurz, S. Grundmann, C. Tropea, M. Forte, A. Seraudie, O. Vermeersch, D. Arnal, R. Goldin, and R. King, "Boundary layer transition control using DBD plasma actuators," Aerosp. Lab (6), p 1–8 (2013).

[5] E. Moreau, A. Debien, J.-M. Breux, and N. Benard, "Control of a turbulent flow separated at mid-chord along an airfoil with DBD plasma actuators," J. Electrostat. **83**, 78–87 (2016).

[6] L. Guoqiang, C. Zhiqiang, Z. Xin, Y. Pengyu, and C. Li, "Experiment on flow control of airfoil dynamic stall using plasma actuator," Acta Aeronaut. Astronaut. Sin. **39**(8), 122111 (2018) (in Chinese).

[7] S. A. Baranova, A. F. Kiseleva, I. A. Moraleva, D. S. Sboev, S. N. Tolkachev, and A. S. L. Chernyshev, "Control of the laminar-turbulent transition in a three-dimensional boundary layer under elevated external turbulence using dielectric barrier discharge," Dokl. Phys. **64**(6), 264–268 (2019).

[8] R. Joussot, R. Weber, A. Leroy, and D. Hong, "Transition control using a single plasma actuator," Int. J. Aerodyn. **3**(1/2/3), 26–46 (2013).

[9] L. Jichun, S. Zhiwei, D. Hai, H. Liang, L. Zheng, and S. Tianwei, "Experimental study of controlling flat transition using surface dielectric barrier discharge actuator," Acta Aeronaut. Astronaut. Sin. **37**(4), 1166–1173 (2016).

[10] S. G. Pouryoussefi, M. Mirzaei, and M. Hajipour, "Experimental study of separation bubble control behind a backward-facing step using plasma actuators," Acta Mech. **226**(4), 1153–1165 (2015).

[11] H. Zare-Behtash and K. Kontisy, "Flow control at subsonic speeds using serpentine plasma actuators," AIAA Paper No. 2014-2812.

[12] W. Bin and L. Huaxing, "Control of flow turbulent kinetic energy by plasma," Acta Aeronaut. Astronaut. Sin. **36**(12), 3809–3821 (2015).

[13] L. Al-Sadawi, T. P. Chong, and J.-H. Kim, "Aerodynamic noise reduction by plasma actuators for a flat plate with blunt trailing edge," J. Sound Vib. **439**, 173–193 (2019).

[14] V. F. Kopiev, P. N. Kazansky, V. A. Kopiev, I. A. Moralev, and M. Y. Zaytsev, "HF DBD plasma actuators for reduction of cylinder noise in flow," J. Phys. D: Appl. Phys. **50**(47), 1 (2017).

[15] H. Zheng, *Research on Vehicle Drag Reduction Based on Plasma Active Flow Control* (College of Automotive Engineering, Jilin University, Changchun, 2020).

[16] H. Xingjun, H. Zheng, G. Peng, Z. Yanghui, Z. Shenshen, G. Yalin, W. Jingyu, and S. Tao, "Experimental investigation into vehicle drag deduction based on plasma flow control," J. South China Univ. Technol. (Nat. Sci. Ed.) **47**(11), 10–15 (2019).

[17] M. Forte, J. Jolibois, J. Pons, E. Moreau, G. Touchard, and M. Cazalens, "Optimization of a dielectric barrier discharge actuator by stationary and non-stationary measurements of the induced flow velocity: Application to airflow control," Exp. Fluids **43**, 917–928 (2007).

[18] F. O. Thomas, T. C. Corke, M. Iqbal, A. Kozlov, and D. Schatzman, "Optimization of dielectric barrier discharge plasma actuators for active aerodynamic flow control," AIAA J. **47**(9), 2169–2178 (2009).

[19] Q. Xiaohua, Y. Liang, Y. Huijie, J. Ying, H. Yue, and R. Chunsheng, "Experimental study on surface dielectric barrier discharge plasma actuator with different encapsulated electrode widths for airflow control at atmospheric pressure," Plasma Sci. Technol. **18**(10), 1005–1011 (2016).

[20] G. Guoqiang, P. Kaisheng, D. Lei, W. Wenfu, and W. Guangning, "Experiment of surface dielectric barrier discharge and aerodynamic characteristics at different voltage amplitude and frequency," Trans. China Electrotech. Soc. **32**(8), 55–62 (2017).

[21] L. Chunmao, D. Lei, P. Kaisheng, W. Wenfu, G. Guoqiang, and W. Guangning, "Influence of electrode gap on characteristics of dielectric barrier discharge," J. Southwest Jiaotong Univ. **54**(4), 679–685 (2019).

[22] W. Ruipeng, X. Yuzhuo, L. Kai, and S. Guoqing, "Orthogonal experiment and univariate analysis in chemical and acoustic co-agglomeration," J. Eng. Therm. Energy Power **35**(10), 103–109 (2020).

[23] Y. Wei, *Research on Thermal Performance Optimization of Microchannel Based on Response Surface Method* (College of Automotive Engineering, Jilin University, Changchun, 2020).

[24] L. Yunyan, *Experiment Design and Data Processing* (Chemical Industry Press, Beijing, 2018).

[25] C. Xueke, N. Wansheng, F. Songjiang, and F. Biming, "Geometrical parameter of dielectric barrier surface discharge," High Voltage Eng. **35**(9), 2213–2219 (2009).

[26] H. Tian-lun, *The Robust Optimization of the Loading Path for T-Shape Tube Hydroforming* (College of Automotive Engineering, Jilin University, Changchun, 2016).